HHS Public Access

Author manuscript

Nano Lett. Author manuscript; available in PMC 2021 October 14.

Published in final edited form as:

Nano Lett. 2020 October 14; 20(10): 7020–7027. doi:10.1021/acs.nanolett.0c01969.

Enhancing surface capture and sensing of proteins with low-power optothermal bubbles in a biphasic liquid

Youngsun Kim[†], **Hongru Ding**[‡], **Yuebing Zheng**[†,‡,*]

[†]Materials Science and Engineering Program and Texas Materials Institute, The University of Texas at Austin, Austin, Texas 78712, USA.

[‡]Walker Department of Mechanical Engineering, The University of Texas at Austin, Austin, Texas 78712, USA.

Abstract

Molecular binding in surface-based biosensing are inherently governed by diffusional transport of molecules in solution to surface-immobilized counterparts. Optothermally generated surface microbubbles can quickly accumulate solutes at the bubble-surface interface due to high-velocity fluid flows. Despite its potential as a concentrator, however, the incorporation of bubbles into protein-based sensing is limited by high temperature. Here, we report a biphasic liquid system, capable of generating microbubbles at low optical power/temperature by formulating PFP as a volatile, water-immiscible component in the aqueous host. We further exploited zwitterionic surface modification to prevent unwanted printing during bubble generation. In a single protein-protein interaction model, surface binding of dispersed antigen to capture antibody was enhanced by one order of magnitude within one minute by bubbles, compared to that from static incubation for 30 min. Our proof-of-concept study exploiting fluid formulation and optothermal add-on paves an effective way towards improving the performances of sensors and spectroscopies.

Graphical Abstract

[*]**Corresponding Author**: zheng@austin.utexas.edu.

Author Contributions

The manuscript was written through contributions of all authors. All authors have given approval to the final version of the manuscript.

Supporting Information.

Experimental methods, photothermal effect on immunobinding affinity of IgG (Figure S1), optical setup (Figure S2), bubble generated in PBS (Figure S3), measured temperature distribution (Figure S4), bubble behavior upon the switching-off of heating laser beam (Figure S5), droplet size-dependent protein accumulation (Figure S6), geometry and temperature distribution in fluid dynamics simulation (Figure S7), size distribution of DPPC liposomes (Figure S8), fluorescence of PFP droplets containing FITC-protein A/G with varying concentration of BSA (Figure S9), physical properties of perfluoropentane and water (Table S1), and Supplementary Note (PDF).

The authors declare no competing financial interest.

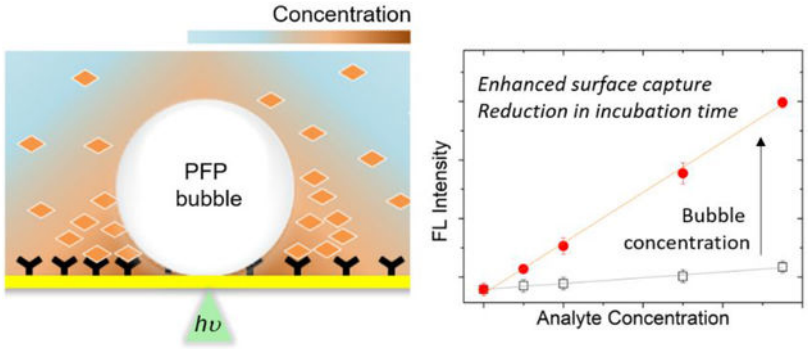

Keywords

Biphasic liquid; microbubbles; Marangoni convection; surface-based biosensing; perfluorocarbon

INTRODUCTION

Surface-based biosensing has been regarded as one of the reliable platforms for the facile separation of analytes and/or probes from solution to solid surface through which surface-confined readout is enabled. Besides optimal pairing of binding species (e.g., surface capture and probe molecules) with molecular/surface designs,[1,2] there have been multifaceted approaches to further improve sensing performance in terms of throughput and sensitivity. Signal amplification strategies in which signal from a single molecular binding event is amplified by enzymes became a gold standard of immunoassay. Nanocatalysts,[3] atom transfer radical polymerization,[4,5] and multiple probes-loaded carriers[6] were exploited in efforts of replacing enzymes or further amplification. On the other hand, color change by growth of plasmonic nanocrystals was shown to be an alternative, sensitive signal-transducing mode for eye detection[7,8]. Apart from the approaches at the signal transduction side, physical concepts have been also utilized at the surface capture/binding step. Binding events in surface-based platforms are governed by passive diffusional transport of suspending molecules (i.e., analytes and/or probes) in the bulk solution toward surface-immobilized capture counterparts in addition to the binding affinity of interacting molecules. In typical sandwich-type enzyme-linked immunosorbent assay (ELISA), each surface binding step takes 30 minutes to an hour, indicating the diffusion-driven incubation process as a time-limiting step. In this context, sensing performance can be improved if the solution is continuously mixed during incubation or the concentration of solutes is conditionally enhanced near surface. Such diffusion-breaking conditions have been demonstrated with several concepts: evaporation of solution on superhydrophobic surface,[9] acoustic streaming, [10] cavitation microstreaming,[11] AC electrokinetics in microfluidic systems,[12] and artificial microswimmer[13] as well as thermo- and electrophoresis-based approaches in a nanopore setting.[14–16]

We have demonstrated the capability of photothermally generated microbubbles to accumulate and print colloidal particles at the bubble-substrate interface through Marangoni convection.[17] The concentration by bubble generation can even induce supersaturation of

ions high enough to enable the crystallization of immiscible metallic nanoalloys.[18] Owing to its fast buildup of strong convective flow based on surface tension gradient and subsequent accumulation of solutes near the substrate, a microbubble is a fascinating candidate as an advanced sensor component for improvements both in time and sensitivity. Biological studies based on the photothermal bubble concentration have been reported for sensing of small molecules[19] and deposition of bacteria.[20,21] However, the application of a bubble-generating scheme to protein-based sensing imposes a major challenge stemming from high temperature (> 100 °C) to generate bubble in the aqueous system. Direct exposure of proteins to such a high temperature, which is inevitable in a typical surface-immobilized sensing scenario, affects the structure of proteins, leading to the loss of their immunobinding properties[22,23] (See Figure S1 for the optothermal effect on the immunobinding property of surface-coated IgG). Given that the denaturation temperature varies among proteins (25–99 °C),[24] the temperature issue will be more critical when proteins with low thermal stability are applied. Although enlarged bubbles, compared to a laser spot diameter, can be used to minimize the thermal damage at the three-phase contact,[20,21] the high temperature required to initiate the bubble generation remains a potential risk in practical surface-based sensing.[25–27]

To overcome this limitation, we hypothesized that a bubble could be optothermally generated at the lower optical power and temperature if volatile liquid droplets suspended in an aqueous medium are present on a plasmonic substrate. Accordingly, criteria for selection of such liquids include low melting point, minimal water miscibility, and inertness toward protein. Among a wide variety of candidates available, attention was given to a material category, called perfluorocarbons (PFCs). PFCs have been considered in the biomedical field as a candidate material for ultrasonography, blood substitute, and liquid breathing due to their bio-inertness, high gas solubility, hydro-/lipophobicity, and/or low boiling point.[28–33] Spurred by these unique material properties along with photothermal control over flow dynamics, we hereby report a biphasic fluid system where PFC droplets are emulsified in an aqueous medium for low-power bubble generation and enhancement of antibody/antigen binding at the substrate driven by bubble-mediated local concentration (Figure 1a,b). Perfluoropentane (C_5F_{12}, PFP) was chosen for its low boiling temperature (~ 30 °C) and high gas solubility as a bubble-generating component. Threshold optical power for bubble generation was reduced to 33% of that in a pure aqueous medium. The generated bubble was able to induce Marangoni flow due to surface tension gradient, which was large enough to accumulate proteins from the bulk solution near the bubble/substrate interface. For the further demonstration of bubble-enhanced protein binding, a plasmonic substrate with a strong optothermal conversion efficiency was modified with zwitterionic molecules in order to address a printing issue (i.e., analytes were unintentionally adsorbed on the substrate) witnessed during the bubble-induced concentration of analytes. One-order-of-magnitude enhancement of surface capture was observed within one minute in a single antigen-antibody model, compared to diffusion-limited incubation for 30 minutes.

RESULTS AND DISCUSSION

Description of bubble generation in the PFP-in-water system.

PFP-in-water emulsion was prepared by adding PFP into the aqueous medium under sonication. As a working buffer for protein, phosphate buffer saline (PBS) was used as the aqueous medium. The fluid system consisted of microscale PFP droplets near the plasmonic substrate with an average size of 1.8 μm, which was estimated from the optical microscopic image (Figure 1c,d). The plasmonic substrate consisted of arrays of gold nanoislands (Au NIs). We observed stationarity of some of the droplet population on the substrate, termed as surface droplets. Other droplets were suspended in a colloidal state throughout the host medium. Surface droplets did not disappear or collapse throughout the duration of monitoring, i.e., around 30 minutes, implying that PFP droplets were stabilized by their high vapor pressure at room temperature[31,34] on the solid surface. A continuous wave laser beam (532 nm in wavelength) was focused on the substrate under the surface droplets to generate a microbubble in a setting of an inverted optical microscope (Figure S2). The threshold optical power density for bubble generation was around 0.26 $mW/\mu m^2$, one third of that in pure PBS (Figure S3), at which the maximum temperature of the substrate reached 36 °C at the laser beam center. The maximum substrate temperature under water-bubble-generating conditions was measured to be higher than 90 °C (Figure S4).

As shown in Figure 2a,b, the growth behavior of bubbles under continuous light exposure has a dependence on the initial size of PFP droplets. While a droplet of 1.4 μm does not evolve to a bubble, droplets larger than 2.0 μm quickly undergo bubble transformation, reaching more than 10 μm within a few seconds upon the light irradiation. After the sharp rise in bubble size, a relative plateau regime was observed with a gradual increase. Similar growth kinetics was observed in droplets of different sizes: larger final bubbles from larger initial droplets. It shall be noted that the bubbles do not collapse upon switching off the heating laser beam (Figure S5).

This droplet-size-dependent bubble growth behavior would originate from intrinsic characteristics of PFP. In particular, PFP exhibits the lower thermal conductivity, the lower heat of vaporization and the higher gas solubility of PFP than water (see Table S1 for physical properties of PFP and water). For bubbles smaller than the critical size, the limited contact area between a PFP droplet and a substrate would drive thermal energy created by the laser-irradiated substrate to be readily dissipated through the water continuum in contact. Note that the laser beam diameter is around 1.0 μm, which is comparable to droplet sizes examined. Above the critical size of PFP droplets (around 2.0 μm) and concomitant critical contact area between PFP and substrate, sufficient heat could accumulate in the basal region of PFP droplets due to low thermal conductivity of PFP, resulting in the onset of vaporization. The initial explosive growth is attributable to high gas solubility and volatile nature of PFP. Assuming that the PFP droplets are air-saturated, the large amounts of air gas (N_2, O_2 and CO_2) dissolved in PFP would contribute to the large expansion of bubbles in addition to PFP vapor once vaporization begins. Moreover, the low heat of vaporization of PFP could accelerate the vaporization of residual liquid PFP within the growing bubble.

The steady state afterwards would be reached by a balance between heat supply from the plasmonic substrate and heat loss through the bubble/liquid interface and by evaporation. Upon the bubble formation, gas molecules in the aqueous phase would be directed toward the bubble-surface interface and taken up by the bubble as suggested in the cases of water[35] and n-alkanes.[36] There would exist a critical bubble diameter above which the mass transfer of gas into the bubble exceeds that out of the bubble.[37,38] Stable bubbles that do not collapse and even slowly grow after light-off may be ascribed to this gas influx.

Bubble-mediated accumulation of proteins at substrate surfaces.

Bubble-mediated concentration of proteins was examined by the time-course measurement of fluorescence intensity near bubbles in PFP-in-water fluid wherein fluorescent proteins are dissolved in the aqueous phase. With a 1.4 μm PFP droplet, fluorescence intensity is indistinguishable from the laser-only signal (Figure 2c,d). Since the droplet of this size does not generate a bubble as seen in the previous section, the possibility of any non-bubble-related accumulation could be excluded. For a 2.0 μm PFP droplet, a sharp rise in the average fluorescence intensity was observed in the initial stage of bubble generation, followed by a gradual increase until 50 seconds of light exposure. These results indicate that the transport of protein from bulk solution to substrate surface occurs quickly at the onset of bubble formation and gradually for the duration of bubble. The degree of protein accumulation was similar in a size range of droplets from 2.0 to 3.6 μm, above which a decreasing trend was observed (Figure S6), implying the limited protein accumulation due to the reduced temperature gradient in larger bubbles. From the simulation shown in Figure 2e, a 15 μm bubble with a temperature difference of 4 K along the bubble-liquid interface is able to build up Marangoni flow with a maximum velocity of 0.04 m/s at the bubble/liquid/solid interfacial region. Please see the Supplementary Note and Figure S7 in the Supporting Information for more details. Although the maximum velocity is much lower than that in pure water (~ 0.3 m/s) with a 60 K temperature difference,[17,39] this biphasic system was capable of delivering and confining proteins to the substrate surface region.

Surface modification to prevent bubble-driven printing of proteins on the substrates.

Another issue in applying the concept of bubble concentration to immunosensing has been direct printing of proteins on the substrate at the three-phase contact line. This phenomenon known as bubble printing or bubble pen lithography was reported in the aqueous medium with micro- and nanoparticles.[17,18] In an ideal case of bubble-enhanced protein-protein interaction, proteins should be concentrated near the substrate by the bubble without any subsequent printing of the proteins on the substrate that could contribute to the background signal. Surface antifouling coating was considered to overcome this challenge. Zwitterionic groups have been proposed as a good candidate for such a coating, in which the presence of positive and negative charges contribute to the formation of a rigid hydration shell and steric hindrance as well as their hydrophilic nature.[40,41]

Among the zwitterions, phosphatidylcholine (PC) as a major component of cell membranes was chosen for our system. Zwitterionic moieties were introduced to gold substrates through a hybrid lipid bilayer membrane that comprises a supporting alkanethiol self-assembled monolayer (SAM) and a cover layer of PC lipid.[42,43] This scheme was adopted because of

the high structural integrity stemming from strong hydrophobic interaction between the two layers as well as strong thiol-gold interaction and minimal fluidity of membranes by highly crystalline SAM.[44] Figure 3a shows the schematic of surface modification and the measured contact angle of the Au NIs substrate with water at each step to verify the modification process. The modification with alkanethiol (hexadecanethiol, HDT) makes the substrate more hydrophobic, increasing the contact angle from 95.4° to 106.9°. After incubation of this substrate with unilamellar liposomes (Figure S8) made of 1,2-dipalmitoyl-sn-glycero-3-phosphocholine (DPPC) and subsequent washing, extremely high hydrophilic surface was obtained, characterized by almost perfect wetting of water. As shown in Figure 3b, the amount of fluorescent proteins that remained on the substrate after bubble concentration and washing was significantly reduced in the DPPC-coated substrate, compared to the unmodified substrate.

Bubble-enhanced surface capture of protein.

As a model to investigate the effects of bubble on surface capturing of proteins, a scheme of direct antigen capture with a single pair of antibody and antigen was adopted. Immunoglobulin G (IgG), a capture antibody, was confined within the lipid layer using biotin-streptavidin conjugation, and FlTC-labeled protein A/G was used as an antigen for its high affinity to IgG and for visualizing the degree of surface binding events (Figure 4a). A concentration range of the antigen was predetermined based on a linear concentration profile after 30 min incubation of the substrate in the solution and subsequent washing, which was considered as a reference. During the preparation of the protein solution, it was found that proteins were localized at the PFP-droplet-water interface, resulting in less availability of free-standing proteins in the solution. We ascribed this phenomenon to the hydrophobicity of proteins. Thus, the final formulation was modified to include bovine serum albumin (BSA), one of the common blocking agents used in immunoassay for reducing nonspecific surface binding. In the presence of BSA with increased concentration, fluorescence intensity from the bulk phase was increased while that from the interface-confined fraction of the droplets was reduced, implying the BSA occupancy on the droplet surfaces (Figure S9). For the bubble-enhanced model, bubbles were optothermally generated from PFP droplets (~ 2.0 μm) at the substrate surface and sustained for 1 minute, followed by repeated washing of the substrate with PBS. As demonstrated in Figure 4b,c, the bubble-concentrated system has a concentration profile that is about nine times steeper than the profile of the diffusion-limited reference system. It was observed that the enhancement factor was almost similar at each protein A/G concentration examined, maintaining the linearity of the concentration profiles for both systems. Furthermore, this bubble-concentrated system has a time-efficient feature where it takes one minute to obtain the enhanced signal in comparison to 30 minutes of incubation in the reference. This result indicates that the local concentration near the surface is effectively amplified by bubble through which the propensity of antigen-antibody collision is increased, eventually leading to the enhanced surface capture as well as reduction in incubation time. In addition to the concentration-driven enhancement of surface capture, there might be partial contribution from the enhanced protein-protein binding reaction by elevated temperature near the bubble.

CONCLUSIONS

A proof-of-concept study on the low-power bubble-generating system and its application as an *in-situ* concentrator for enhancing surface capture of proteins has been demonstrated. The formulation of volatile and water-immiscible liquid phase into the aqueous host medium was found to effectively reduce the optical power threshold for bubble generation, enabling the bulk-to-substrate accumulation of proteins with minimal thermal deterioration of protein's activity. The bubble growth behavior could be explained in terms of intrinsic properties of PFP. Together with zwitterionic surface modification, the low-power bubble generation was able to improve the capture efficiency of proteins by one order of magnitude in sensitivity and by 30-fold reduction in time, compared to a diffusion-limited setting.

One of the merits of the bubble-based approach, composed of fluid formulation and an optothermal add-on, resides in its compatibility with conventional surface-based assay platforms. Given the working mode of our concept, the same method can be sequentially applied to multiple steps of solution-to-surface conjugation as in sandwich-type ELISA, e.g., capture antibody/antigen, antigen/probe antibody, probe antibody/secondary antibody, and enzyme/substrate. Collective improvement of its performance in sensitivity and throughput can be expected from enhancements in binding events at each step. To maximize the practical capacity of the presented concept, size uniformity of droplets may be further improved by fluorosurfactants,[45,46] along with uniform placement of droplets throughout a substrate assisted by pre-defined micropatterns.[20] The present study will find a wider range of scientific and clinical applications when combined with rational designs of sensor configuration, as well as suggesting a way toward improving the performances of sensors and spectroscopies.

Supplementary Material

Refer to Web version on PubMed Central for supplementary material.

ACKNOWLEDGMENT

The authors acknowledge the financial supports of the National Science Foundation (NSF-CMMI-1761743), the National Aeronautics and Space Administration Early Career Faculty Award (80NSSC17K0520), and the National Institute of General Medical Sciences of the National Institutes of Health (DP2GM128446). We acknowledge Pavana S. Kollipara for helpful discussion on the numerical simulation.

REFERENCES

(1). Nakatsuka N; Cao HH; Deshayes S; Melkonian AL; Kasko AM; Weiss PS; Andrews AM Aptamer Recognition of Multiplexed Small-Molecule-Functionalized Substrates. ACS Appl. Mater. Interfaces 2018, 10 (28), 23490–23500. 10.1021/acsami.8b02837. [PubMed: 29851335]

(2). Vaish A; Shuster MJ; Cheunkar S; Singh YS; Weiss PS; Andrews AM Native Serotonin Membrane Receptors Recognize 5-Hydroxytryptophan-Functionalized Substrates: Enabling Small-Molecule Recognition. ACS Chem. Neurosci 2010, 1 (7), 495–504. 10.1021/cn1000205. [PubMed: 22778841]

(3). Loynachan CN; Thomas MR; Gray ER; Richards DA; Kim J; Miller BS; Brookes JC; Agarwal S; Chudasama V; McKendry RA; Stevens MM Platinum Nanocatalyst Amplification: Redefining the Gold Standard for Lateral Flow Immunoassays with Ultrabroad Dynamic Range. ACS Nano 2018, 12 (1), 279–288. 10.1021/acsnano.7b06229. [PubMed: 29215864]

(4). Liu Y; Cheng Q Detection of Membrane-Binding Proteins by Surface Plasmon Resonance with an All-Aqueous Amplification Scheme. Anal. Chem 2012, 84 (7), 3179–3186. 10.1021/ac203142n. [PubMed: 22439623]

(5). Yuan L; Xu L; Liu S Integrated Tyramide and Polymerization-Assisted Signal Amplification for a Highly-Sensitive Immunoassay. Anal. Chem 2012, 84 (24), 10737–10744. 10.1021/ac302439v. [PubMed: 23181414]

(6). Chikkaveeraiah BV; Mani V; Patel V; Gutkind JS; Rusling JF Microfluidic Electrochemical Immunoarray for Ultrasensitive Detection of Two Cancer Biomarker Proteins in Serum. Biosens. Bioelectron 2011, 26 (11), 4477–4483. 10.1016/j.bios.2011.05.005. [PubMed: 21632234]

(7). Rodríguez-Lorenzo L; De La Rica R; Álvarez-Puebla RA; Liz-Marzán LM; Stevens MM Plasmonic Nanosensors with Inverse Sensitivity by Means of Enzyme-Guided Crystal Growth. Nat. Mater 2012, 11 (7), 604–607. 10.1038/nmat3337. [PubMed: 22635043]

(8). De La Rica R; Stevens MM Plasmonic ELISA for the Ultrasensitive Detection of Disease Biomarkers with the Naked Eye. Nat. Nanotechnol 2012, 7 (12), 821–824. 10.1038/nnano.2012.186. [PubMed: 23103935]

(9). De Angelis F; Gentile F; Mecarini F; Das G; Moretti M; Candeloro P; Coluccio ML; Cojoc G; Accardo A; Liberale C; Zaccaria RP; Perozziello G; Tirinato L; Toma A; Cuda G; Cingolani R; Di Fabrizio E Breaking the Diffusion Limit with Super-Hydrophobic Delivery of Molecules to Plasmonic Nanofocusing SERS Structures. Nat. Photonics 2011, 5 (11), 682–687. 10.1038/nphoton.2011.222.

(10). Maturos T; Pogfay T; Rodaree K; Chaotheing S; Jomphoak A; Wisitsoraat A; Suwanakitti N; Wongsombat C; Jaruwongrungsee K; Shaw P; Kamchonwongpaisan S; Tuantranont A Enhancement of DNA Hybridization under Acoustic Streaming with Three-Piezoelectric-Transducer System. Lab Chip 2012, 12 (1), 133–138. 10.1039/c1lc20720b. [PubMed: 22072313]

(11). Liu RH; Lenigk R; Druyor-Sanchez RL; Yang J; Grodzinski P Hybridization Enhancement Using Cavitation Microstreaming. Anal. Chem 2003, 75 (8), 1911–1917. 10.1021/ac026267t. [PubMed: 12713050]

(12). Liu X; Yang K; Wadhwa A; Eda S; Li S; Wu J Development of an AC Electrokinetics-Based Immunoassay System for on-Site Serodiagnosis of Infectious Diseases. Sensors Actuators A Phys. 2011, 171 (2), 406–413. 10.1016/j.sna.2011.08.007.

(13). Morales-Narváez E; Guix M; Medina-Sánchez M; Mayorga-Martinez CC; Merkoçi A Micromotor Enhanced Microarray Technology for Protein Detection. Small 2014, 10 (13), 2542–2548. 10.1002/smll.201303068. [PubMed: 24634101]

(14). Nicoli F; Verschueren D; Klein M; Dekker C; Jonsson MP DNA Translocations through Solid-State Plasmonic Nanopores. Nano Lett. 2014, 14 (12), 6917–6925. 10.1021/nl503034j. [PubMed: 25347403]

(15). Crick CR; Albella P; Kim HJ; Ivanov AP; Kim KB; Maier SA; Edel JB Low-Noise Plasmonic Nanopore Biosensors for Single Molecule Detection at Elevated Temperatures. ACS Photonics 2017, 4 (11), 2835–2842. 10.1021/acsphotonics.7b00825.

(16). Shi X; Verschueren DV; Dekker C Active Delivery of Single DNA Molecules into a Plasmonic Nanopore for Label-Free Optical Sensing. Nano Lett. 2018, 18 (12), 8003–8010. 10.1021/acs.nanolett.8b04146. [PubMed: 30460853]

(17). Lin L; Peng X; Mao Z; Li W; Yogeesh MN; Rajeeva BB; Perillo EP; Dunn AK; Akinwande D; Zheng Y Bubble-Pen Lithography. Nano Lett. 2016, 16 (1), 701–708. 10.1021/acs.nanolett.5b04524. [PubMed: 26678845]

(18). Rajeeva BB; Kunal P; Kollipara PS; Acharya PV; Joe M; Ide MS; Jarvis K; Liu Y; Bahadur V; Humphrey SM; Zheng Y Accumulation-Driven Unified Spatiotemporal Synthesis and Structuring of Immiscible Metallic Nanoalloys. Matter 2019, 1 (6), 1606–1617. 10.1016/j.matt.2019.10.017.

(19). Karim F; Vasquez ES; Sun Y; Zhao C Optothermal Microbubble Assisted Manufacturing of Nanogap-Rich Structures for Active Chemical Sensing. Nanoscale 2019, 11 (43), 20589–20597. 10.1039/C9NR05892C. [PubMed: 31638631]

(20). Tokonami S; Kurita S; Yoshikawa R; Sakurai K; Suehiro T; Yamamoto Y; Tamura M; Karthaus O; Iida T Light-Induced Assembly of Living Bacteria with Honeycomb Substrate. Sci. Adv 2020, 6 (9). 10.1126/sciadv.aaz5757.

(21). Yamamoto Y; Tokonami S; Iida T Surfactant-Controlled Photothermal Assembly of Nanoparticles and Microparticles for Rapid Concentration Measurement of Microbes. ACS Appl. Bio Mater 2019, 2 (4), 1561–1568. 10.1021/acsabm.8b00838.

(22). Wang J; Yiu B; Obermeyer J; Filipe CDM; Brennan JD; Pelton R Effects of Temperature and Relative Humidity on the Stability of Paper-Immobilized Antibodies. Biomacromolecules 2012, 13 (2), 559–564. 10.1021/bm2017405. [PubMed: 22257068]

(23). Wang W; Singh S; Zeng DL; King K; Nema S Antibody Structure, Instability, and Formulation. J. Pharm. Sci 2007, 96 (1), 1–26. 10.1002/jps.20727. [PubMed: 16998873]

(24). Ku T; Lu P; Chan C; Wang T; Lai S; Lyu P; Hsiao N Predicting Melting Temperature Directly from Protein Sequences. Comput. Biol. Chem 2009, 33 (6), 445–450. 10.1016/j.compbiolchem.2009.10.002. [PubMed: 19896904]

(25). Xie Y; Zhao C An Optothermally Generated Surface Bubble and Its Applications. Nanoscale 2017, 9 (20), 6622–6631. 10.1039/C7NR01360D. [PubMed: 28485456]

(26). Tantussi F; Messina GC; Capozza R; Dipalo M; Lovato L; De Angelis F Long-Range Capture and Delivery of Water-Dispersed Nano-Objects by Microbubbles Generated on 3D Plasmonic Surfaces. ACS Nano 2018, 12 (5), 4116–4122. 10.1021/acsnano.7b07893. [PubMed: 29589906]

(27). Moon S; Zhang Q; Huang D; Senapati S; Chang HC; Lee E; Luo T Biocompatible Direct Deposition of Functionalized Nanoparticles Using Shrinking Surface Plasmonic Bubble. Adv. Mater. Interfaces 2020, 2000597, 1–8. 10.1002/admi.202000597.

(28). Lin C-Y; Javadi M; Belnap DM; Barrow JR; Pitt WG Ultrasound Sensitive ELiposomes Containing Doxorubicin for Drug Targeting Therapy. Nanomedicine Nanotechnology, Biol. Med 2014, 10 (1), 67–76. 10.1016/j.nano.2013.06.011.

(29). Yang P; Li D; Jin S; Ding J; Guo J; Shi W; Wang C Stimuli-Responsive Biodegradable Poly(Methacrylic Acid) Based Nanocapsules for Ultrasound Traced and Triggered Drug Delivery System. Biomaterials 2014, 35 (6), 2079–2088. 10.1016/j.biomaterials.2013.11.057. [PubMed: 24331704]

(30). Díaz-López R; Tsapis N; Fattal E Liquid Perfluorocarbons as Contrast Agents for Ultrasonography and 19F-MRI. Pharm. Res 2010, 27 (1), 1–16. 10.1007/s11095-009-0001-5. [PubMed: 19902338]

(31). Riess JG Understanding the Fundamentals of Perfluorocarbons and Perfluorocarbon Emulsions Relevant to In Vivo Oxygen Delivery. Artif. Cells, Blood Substitutes, Biotechnol 2005, 33 (1), 47–63. 10.1081/BIO-200046659.

(32). Rapoport N; Nam K-H; Gupta R; Gao Z; Mohan P; Payne A; Todd N; Liu X; Kim T; Shea J; Scaife C; Parker DL; Jeong E-K; Kennedy AM Ultrasound-Mediated Tumor Imaging and Nanotherapy Using Drug Loaded, Block Copolymer Stabilized Perfluorocarbon Nanoemulsions. J. Control. Release 2011, 153 (1), 4–15. 10.1016/j.jconrel.2011.01.022. [PubMed: 21277919]

(33). Cosco D; Fattal E; Fresta M; Tsapis N Perfluorocarbon-Loaded Micro and Nanosystems for Medical Imaging: A State of the Art. J. Fluor. Chem 2015, 171, 18–26. 10.1016/j.jfluchem.2014.10.013.

(34). Schutt EG; Klein DH; Mattrey RM; Riess JG Injectable Microbubbles as Contrast Agents for Diagnostic Ultrasound Imaging: The Key Role of Perfluorochemicals. Angew. Chemie - Int. Ed 2003, 42 (28), 3218–3235. 10.1002/anie.200200550.

(35). Wang Y; Zaytsev ME; The H. Le; Eijkel JCT; Zandvliet HJW; Zhang X; Lohse D Vapor and Gas-Bubble Growth Dynamics around Laser-Irradiated, Water-Immersed Plasmonic Nanoparticles. ACS Nano 2017, 11 (2), 2045–2051. 10.1021/acsnano.6b08229. [PubMed: 28088847]

(36). Zaytsev ME; Lajoinie G; Wang Y; Lohse D; Zandvliet HJW; Zhang X Plasmonic Bubbles in N-Alkanes. J. Phys. Chem. C 2018, 122 (49), 28375–28381. 10.1021/acs.jpcc.8b09617.

(37). Ward CA; Tikuisis P; Venter RD Stability of Bubbles in a Closed Volume of Liquid-gas Solution. J. Appl. Phys 1982, 53 (9), 6076–6084. 10.1063/1.331559.

(38). Ward CA; Levart E Conditions for Stability of Bubble Nuclei in Solid Surfaces Contacting a Liquid-gas Solution. J. Appl. Phys 1984, 56 (2), 491–500. 10.1063/1.333937.

(39). Kotnala A; Kollipara PS; Li J; Zheng Y Overcoming Diffusion-Limited Trapping in Nanoaperture Tweezers Using Opto-Thermal-Induced Flow. Nano Lett. 2020, 20 (1), 768–779. 10.1021/acs.nanolett.9b04876. [PubMed: 31834809]

(40). He M; Gao K; Zhou L; Jiao Z; Wu M; Cao J; You X; Cai Z; Su Y; Jiang Z Zwitterionic Materials for Antifouling Membrane Surface Construction. Acta Biomater. 2016, 40 (92), 142–152. 10.1016/j.actbio.2016.03.038. [PubMed: 27025359]

(41). Schlenoff JB Zwitteration: Coating Surfaces with Zwitterionic Functionality to Reduce Nonspecific Adsorption. Langmuir 2014, 30 (32), 9625–9636. 10.1021/la500057j. [PubMed: 24754399]

(42). Plant AL Self-Assembled Phospholipid/Alkanethiol Biomimetic Bilayers on Gold. Langmuir 1993, 9 (11), 2764–2767. 10.1021/la00035a004.

(43). Plant AL; Brighamburke M; Petrella EC; Oshannessy DJ Phospholipid/Alkanethiol Bilayers for Cell-Surface Receptor Studies by Surface Plasmon Resonance. Anal. Biochem 1995, 226 (2), 342–348. 10.1006/abio.1995.1234. [PubMed: 7793636]

(44). Khan MS; Dosoky NS; Williams JD Engineering Lipid Bilayer Membranes for Protein Studies. Int. J. Mol. Sci 2013, 14 (11), 21561–21597. 10.3390/ijms141121561. [PubMed: 24185908]

(45). Fernandes DA; Fernandes DD; Li Y; Wang Y; Zhang Z; Rousseau D; Gradinaru CC; Kolios MC Synthesis of Stable Multifunctional Perfluorocarbon Nanoemulsions for Cancer Therapy and Imaging. Langmuir 2016, 32 (42), 10870–10880. 10.1021/acs.langmuir.6b01867. [PubMed: 27564412]

(46). Zarzar LD; Sresht V; Sletten EM; Kalow JA; Blankschtein D; Swager TM Dynamically Reconfigurable Complex Emulsions via Tunable Interfacial Tensions. Nature 2015, 518 (7540), 520–524. 10.1038/nature14168. [PubMed: 25719669]

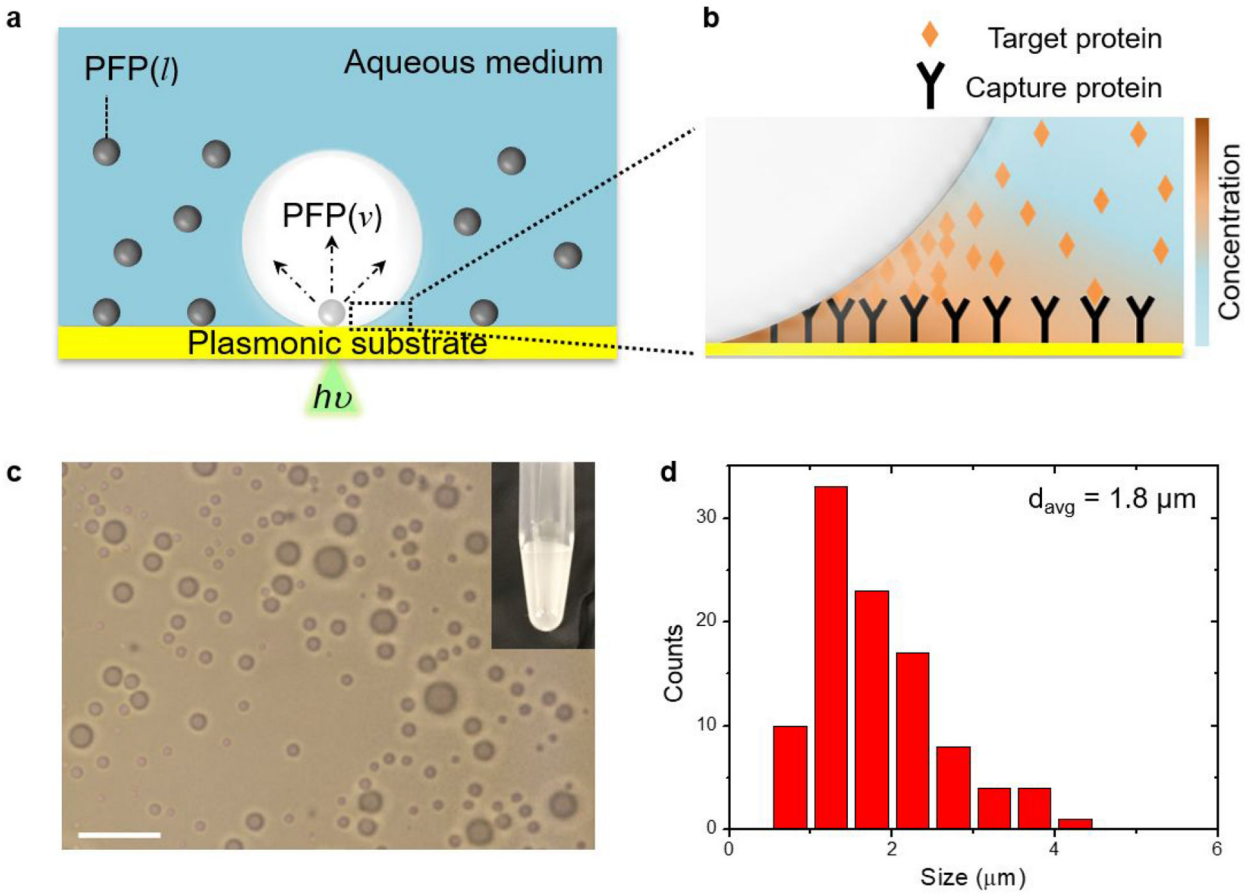

Figure 1. Scheme of bubble-enhanced surface capture of proteins and description of biphasic fluid.

(a) Schematic illustration of the bubble-generating PFP-in-water system and (B) bubble-mediated concentration of target proteins near the bubble/substrate interface. Arrows in (a) indicate the expansion of the PFP droplet into the bubble. (c) Optical image of PFP droplets (scale bar: 10 μm). Inset of (c) is a photograph of PFP-in-water fluid. (d) Size distribution of PFP droplets with a total number n=100.

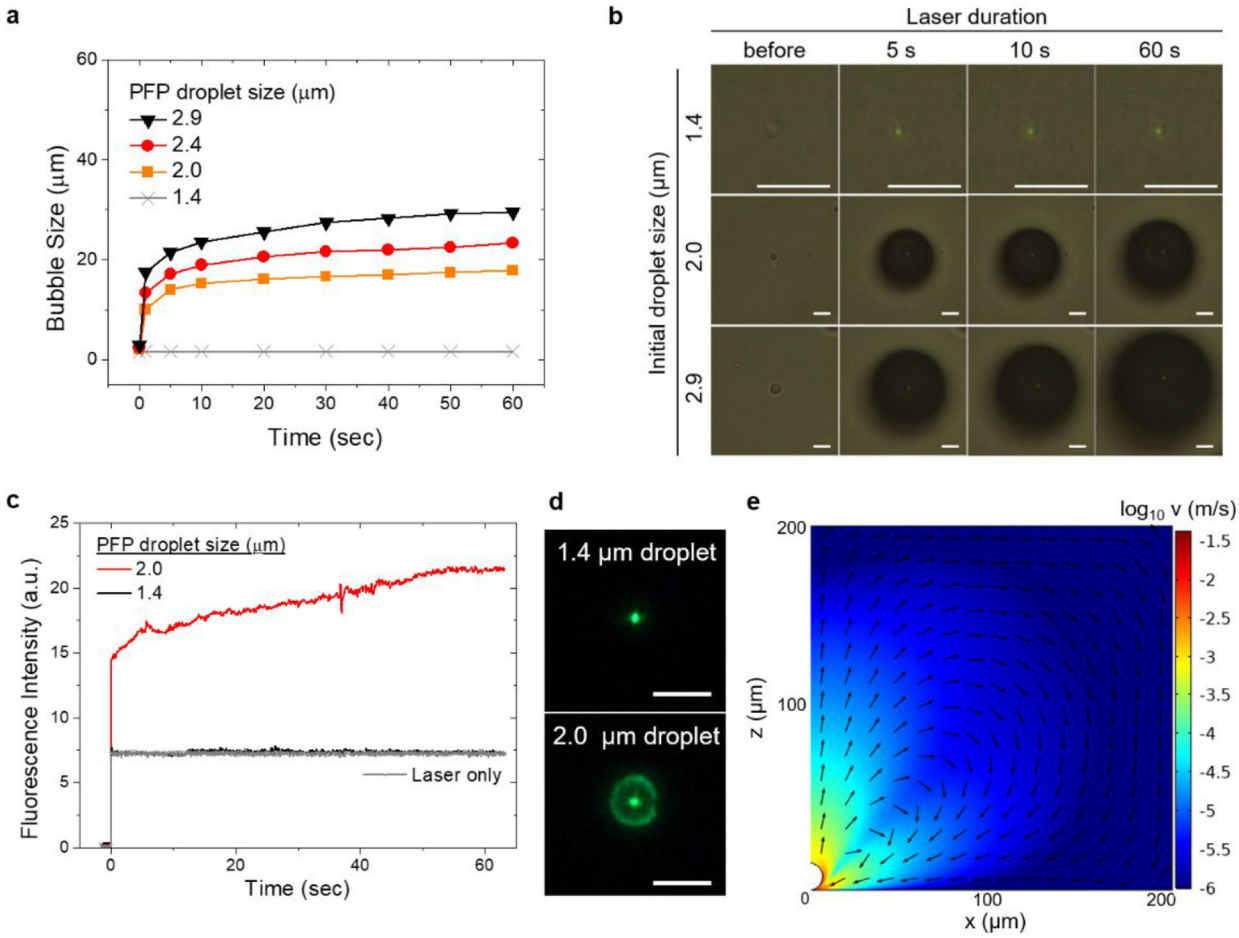

Figure 2. Bubble generation and concentration of protein.

(a) Growth behavior of bubbles arising from PFP droplets with different diameters. (b) A series of optical images showing the evolution of bubbles arising from PFP droplets with different diameters (scale bar: 5 μm). (c) Temporal evolution of fluorescence intensity (FITC-anti rabbit IgG, 10 μg/mL in PBS) around the laser spot for two PFP droplets of different sizes and (d) corresponding fluorescence images after 60 seconds of bubble duration (scale bar: 5 μm). The zero timepoint indicates the light incident. Fluorescence intensity was measured from the defined region of interest around the laser spot. (e) Simulated velocity profile near the 15 μm bubble. Arrows indicate normalized velocity.

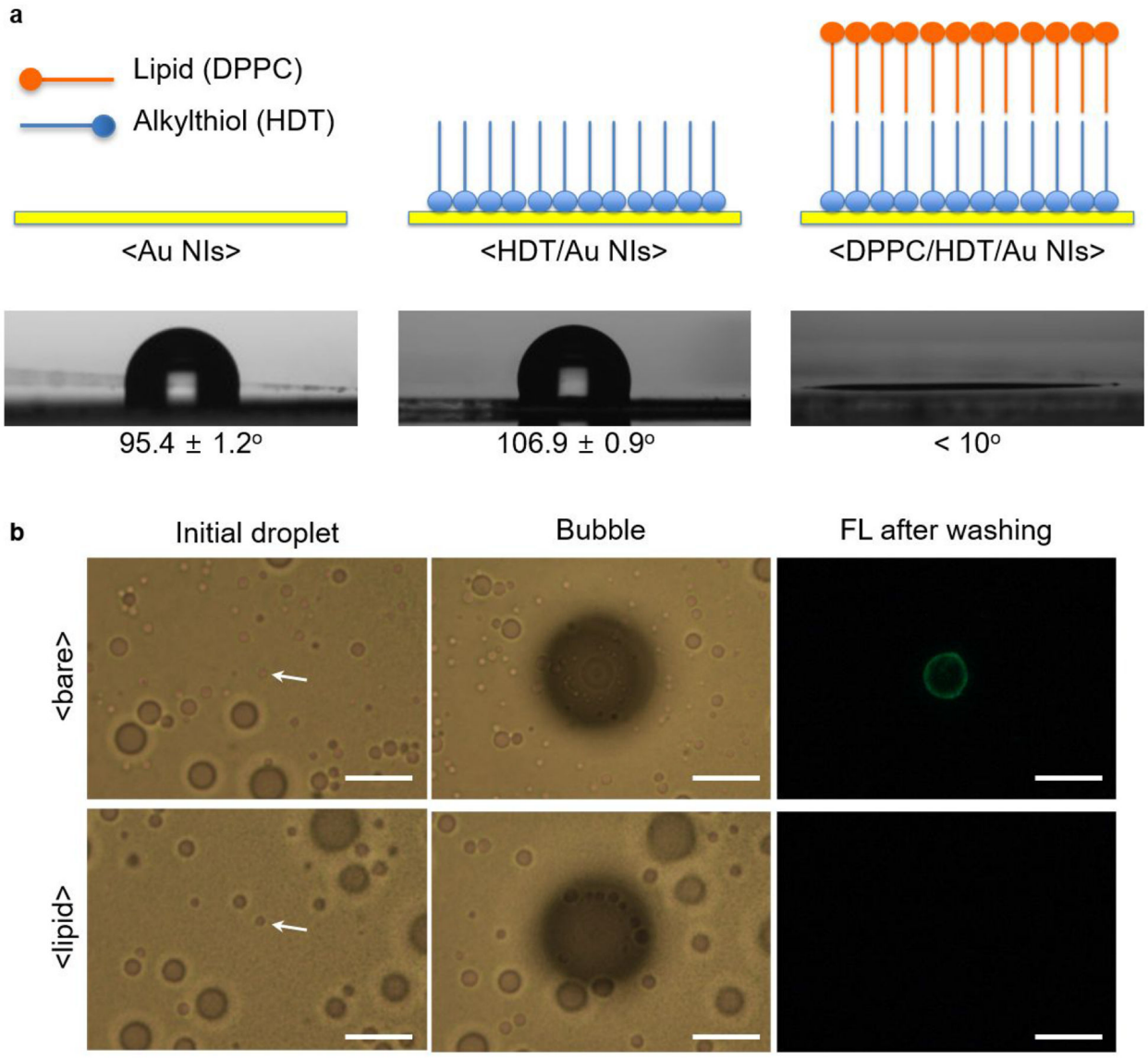

Figure 3. Zwitterionic surface modification to reduce bubble printing of proteins.

(a) Schematic illustration of surface-modified Au NIs and their contact angle with a water droplet (3 μL) at each modification step. (b) Optical images of initial droplets and generated bubbles, and fluorescence images of substrates after bubble concentration of fluorescent proteins (FITC-anti rabbit IgG, 10 μg/mL) for 1 min and subsequent washing (scale bars: 10 μm). Top row is for bare Au NI substrate as indicated by <bare>. Bottom row is for the DPPC-coated substrate as indicated by <lipid>.

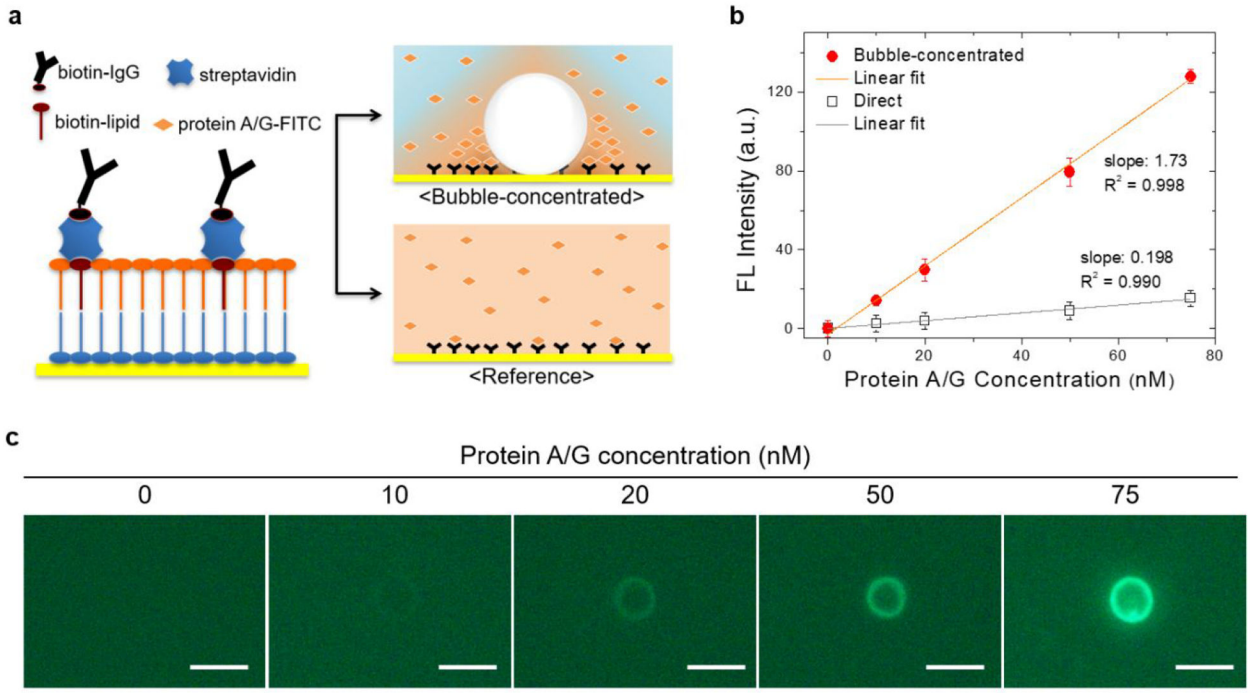

Figure 4. Bubble-enhanced surface capture of proteins.

(A) Schematic diagrams of surface immobilization of capture protein and two assay models: (i) bubble-concentrated and (ii) diffusion-limited incubation as reference. (B) Surface binding profile of FITC-protein A/G in the bubble-concentrated model (bubble concentration for 1 min) in comparison to the reference (incubation for 30 min). Fluorescence intensity in the bubble-concentrated model is the average of peak intensity at the ring patterns (n=3, individual bubble generation), and background intensity was subtracted. (C) Fluorescence images of substrates after the bubble concentration of FITC-protein A/G at varying concentration, i.e., 0, 10, 20, 50, and 75 nM (scale bar: 5 μm).